Supplementary Figures

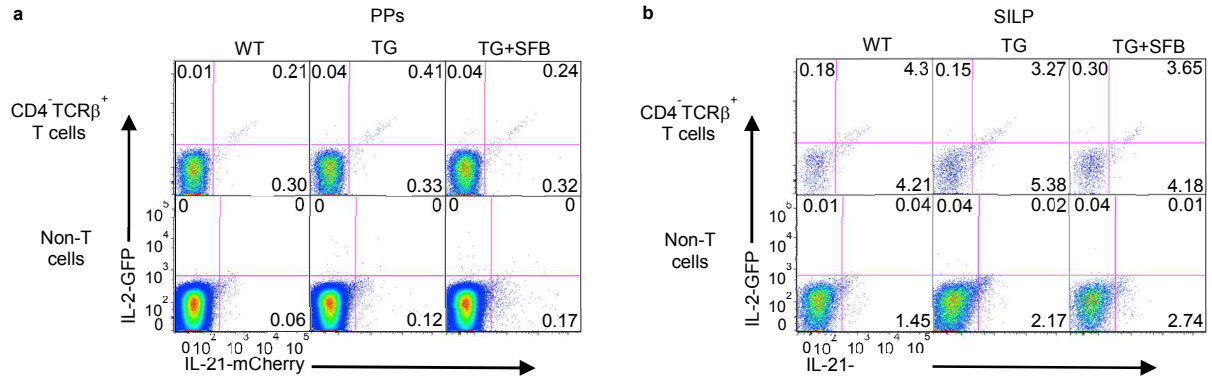

Supplementary Figure 1. IL-21 production from CD4$^-$TCRβ$^+$ and non-T cells. Related to Fig. 1. **a, b**, IL-21-mCherry expression in non-CD4 T cells isolated from PP (**a**) and SILP (**b**) of WT, TG, or TG mice co-housed with SFB$^+$ mice. "Non-T cells" means all of the remaining cells after gating out TCRβ$^+$ cells. Representative of 2 independent experiments.

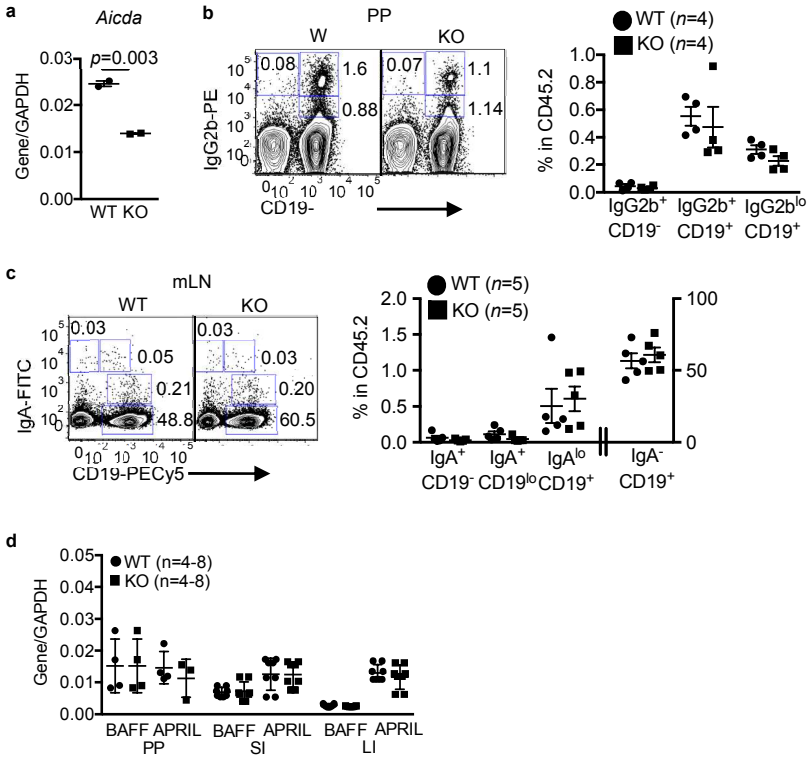

Supplementary Figure 2. Normal Peyer's patch IgG2b$^+$ and mesenteric LN IgA$^+$ B cell populations in SFB$^+$ IL-21R KO mice. Related to Fig. 2. **a,** *Aicda* mRNA expression in sorted PP IgA$^-$CD19$^+$ B cells from SFB$^+$ mice measured by real-time RT-PCR. Shown is one of 2 similar experiments. **b**, Intracellular IgG2b staining of PP B cells gated on CD45.2$^+$. The graphs indicate the frequency of various IgG2b B cell populations. Data were combined from 2 independent experiments. **c**, Intracellular IgA staining of mLN B cells gated on CD45.2$^+$. The graph indicates the frequency of various IgA B cell populations. Data were compiled from 2 independent experiments. **d**, Expression of BAFF and APRIL mRNAs in various organs. Data are represented as mean ± SEM.

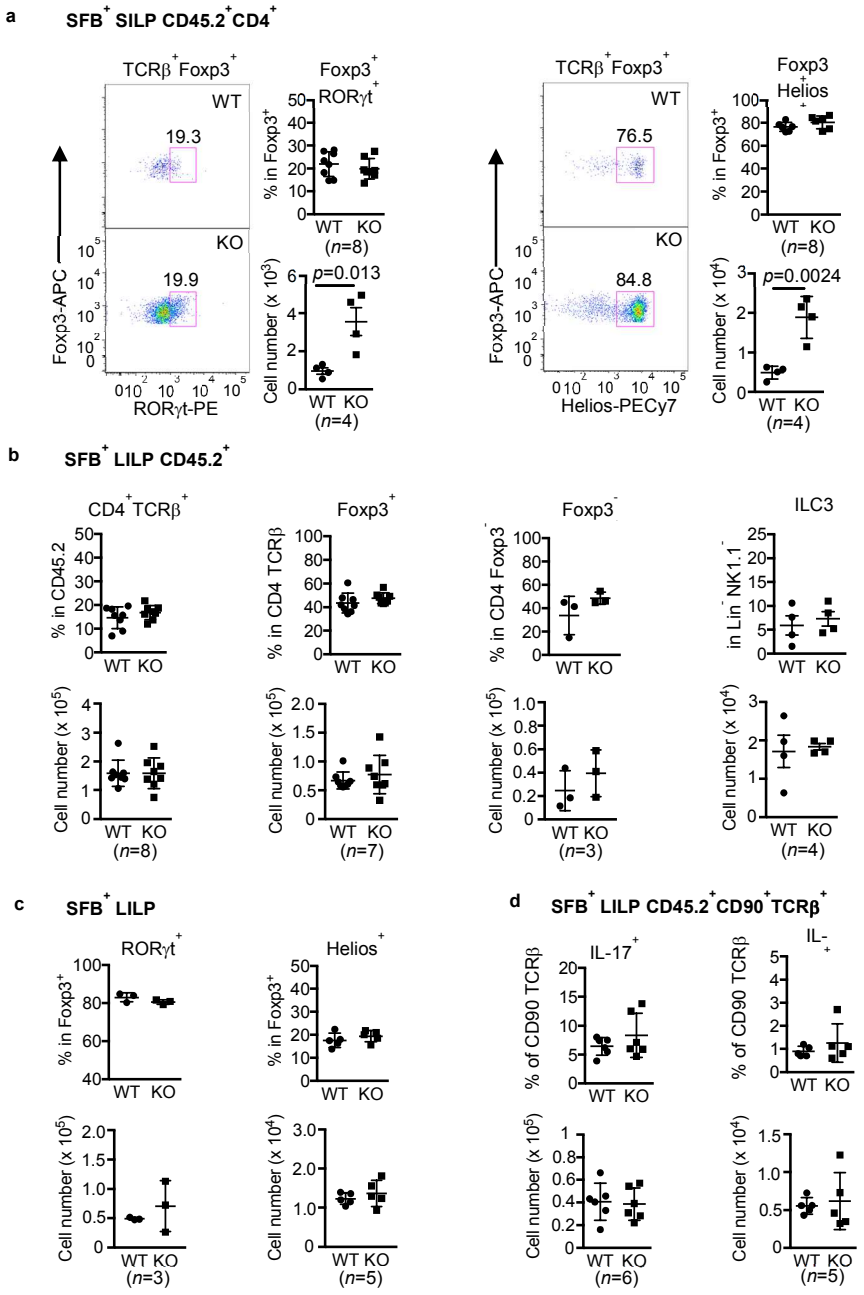

Supplementary Figure 3. Comparison of SILP Treg cells and LILP T cells and ILC3 from SFB$^+$ WT and IL-21R KO. Related to Fig. 4. **a**, SILP Treg cells were further gated based on their RORγt or Helios expression. The graphs indicate the frequency and cell number of RORγt$^+$ or Helios$^+$ Treg cells. **b-d**, LILP cell populations. The same gating strategies described in Fig. 4 were used. The graphs indicate the frequency and cell number of various cell types. Data summarize 2-4 independent experiments and are represented as mean ± SEM.

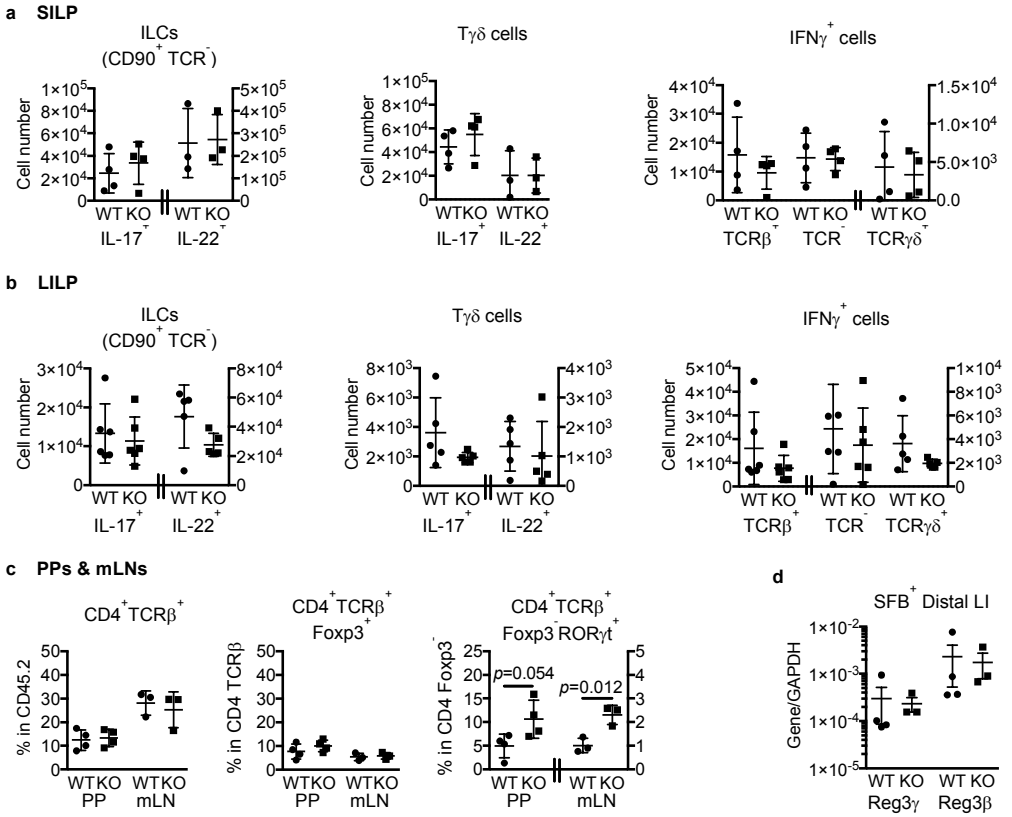

Supplementary Figure 4. IL-17$^+$, IL-22$^+$, and IFNγ$^+$ cells in SILP and LILP and T cells in Peyer's patches and mesenteric LNs of SFB$^+$ WT and IL-21R KO mice. Related to Fig. 4. **a, b**, The numbers of IL-17$^+$, IL-22$^+$, and IFNγ$^+$ cell populations in SILP (**a**) and LILP (**b**). Cells were stimulated *in vitro* with PMA and ionomycin for 4 hours (a pool of 2 mice). IL-22$^+$ includes both IL-22 single-positive and IL-17/IL-22 double-positive cells. **c**, Frequencies of various T cells in PPs and mLNs. **d**, Expression of Reg3γ and Reg3β in the distal colon of SFB$^+$ WT and IL-21R KO mice (Related to Fig. 5**a**). Data summarize 2-4 independent experiments and are represented as mean ± SEM.

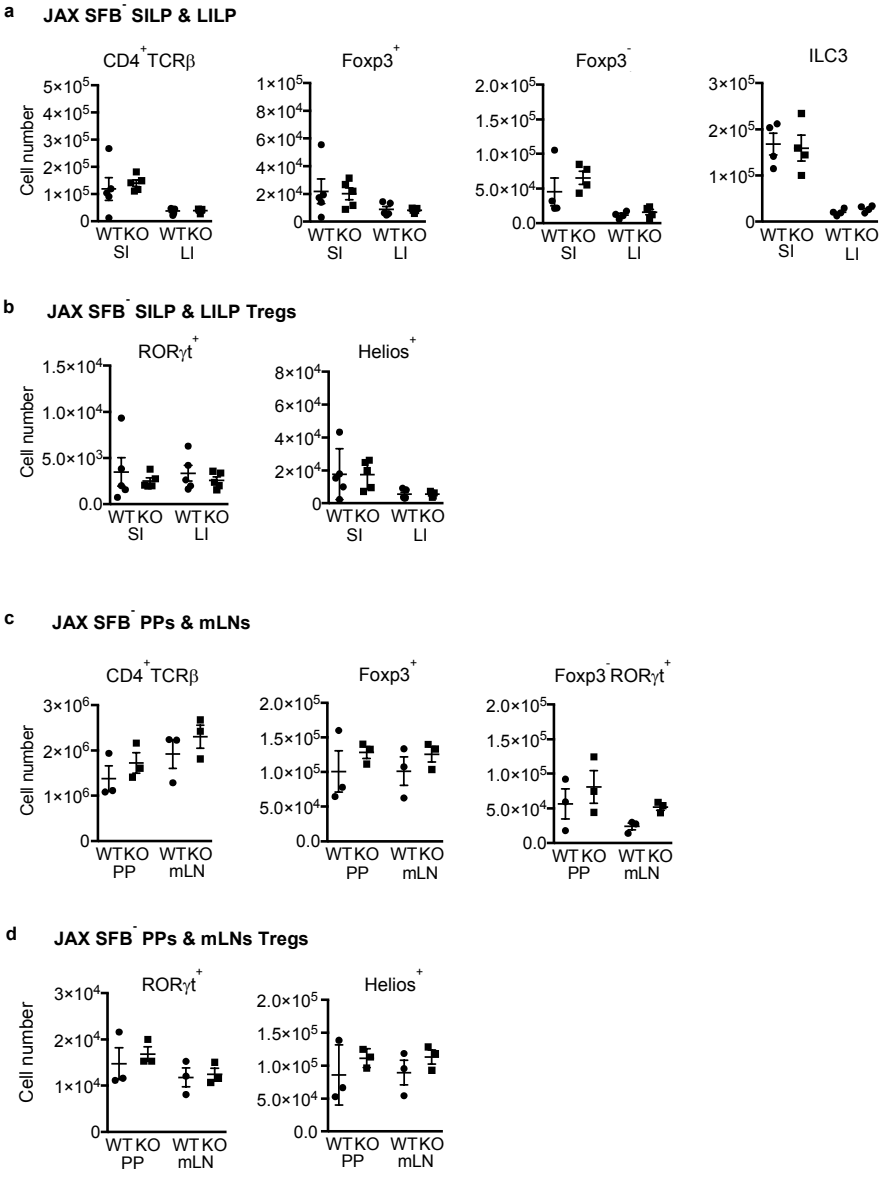

Supplementary Figure 5. Tregs, Th17 cells, and ILC3 in the intestine of SFB$^-$ IL-21R KO mice. Related to Fig. 4. **a, b**, The numbers of CD4$^+$TCRβ$^+$ T cells, Foxp3$^+$ Tregs, RORγt$^+$ Th17 cells, and ILC3s (**a**) as well as RORγt$^+$ and Helios$^+$ Treg cells (**b**) isolated from the SILP and LILP of SFB$^-$ WT and IL-21R KO mice. **c, d**, The numbers of CD4$^+$TCRβ$^+$ T cells, Foxp3$^+$ Tregs, and RORγt$^+$ Th17 cells (**c**) as well as RORγt$^+$ and Helios$^+$ Treg cells (**d**) from the PPs and mLNs of SFB$^-$ WT and IL-21R KO mice. Data summarize 2 independent experiments and are represented as mean ± SEM.

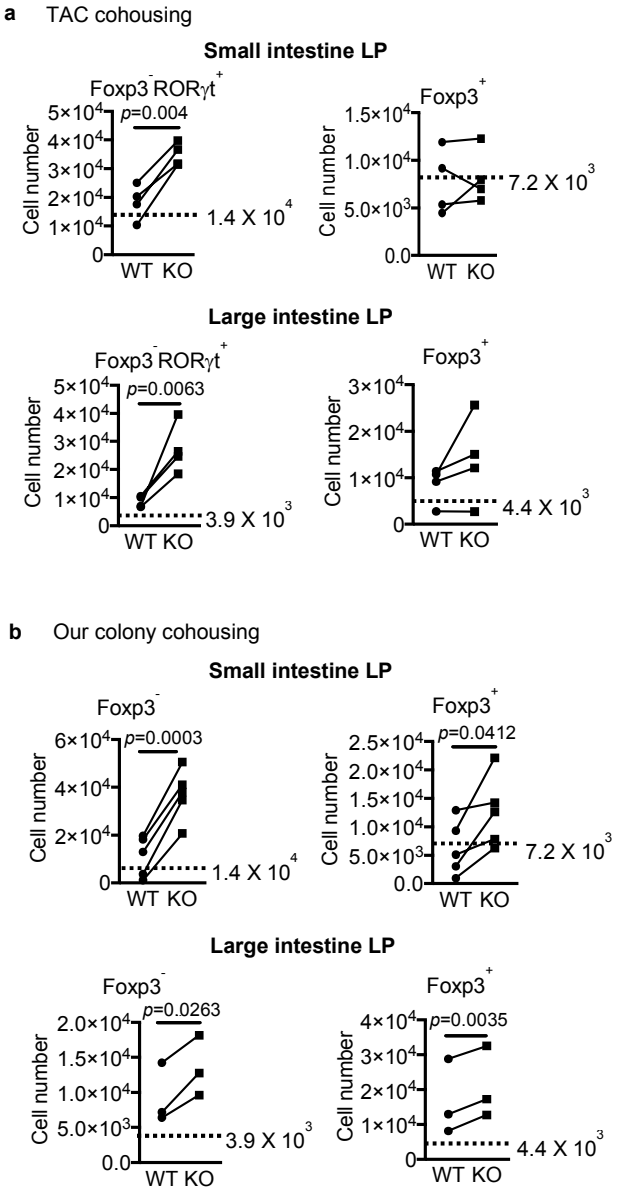

Supplementary Figure 6. Co-housing experiment. SFB$^-$ littermate WT and IL-21R KO mice were co-housed with either SFB$^+$ mice from Taconic Farm (**a**) or with SFB$^+$ mice from our IL-21R breeding colonies (**b**) for 4 weeks. The cell numbers of Foxp3$^-$RORγt$^+$ and Foxp3$^+$ CD4 T cells isolated from the SILP and LILP are shown. The before-after line plot indicates SFB$^-$ WT and IL-21R KO mice housed in the same cage. The dotted line with the number indicates the average cell number of four non-cohoused SFB$^-$ WT mice. Data sumarize 2 independent experiments and are represented as mean ± SEM.

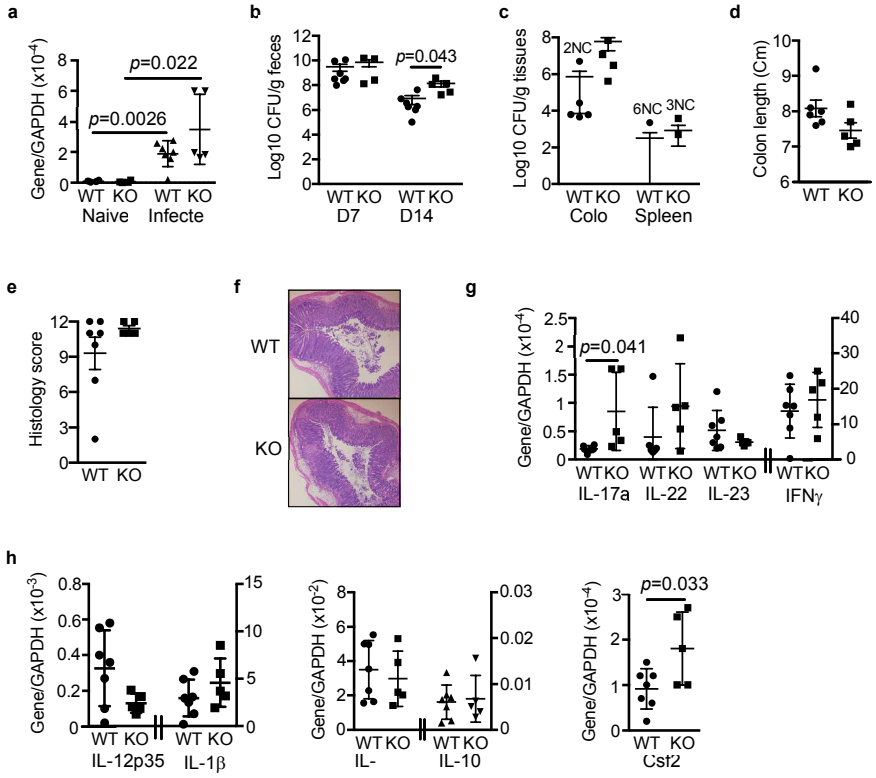

Supplementary Figure 7. *C. rodentium* infection with SFB$^-$ IL-21R KO mice. Related to Fig. 7. **a**, IL-21 mRNA levels in the distal colon of naïve mice and mice orally inoculated with *C. rodentium* (~2 x 10^9 CFU) at day 14 post-infection (pi). **b**, *C. rodentium* burden in the feces on day 7 (D7) and 14 (D14) pi. **c**, *C. rodentium* burden in the distal colon and spleen on D14 pi. NC stands for no colonies observed. **d**, Colon length on D14 pi. **e**, Histology score of distal colon on D14 pi. **f**, A representative H& E staining of distal colon. **g, h**, Expression of various cytokine mRNAs by real-time RT-PCR in the distal colon on D14 pi. Data were compiled from 2 independent experiments (WT; *n*=7, KO; *n*=5) and are represented as mean ± SEM.

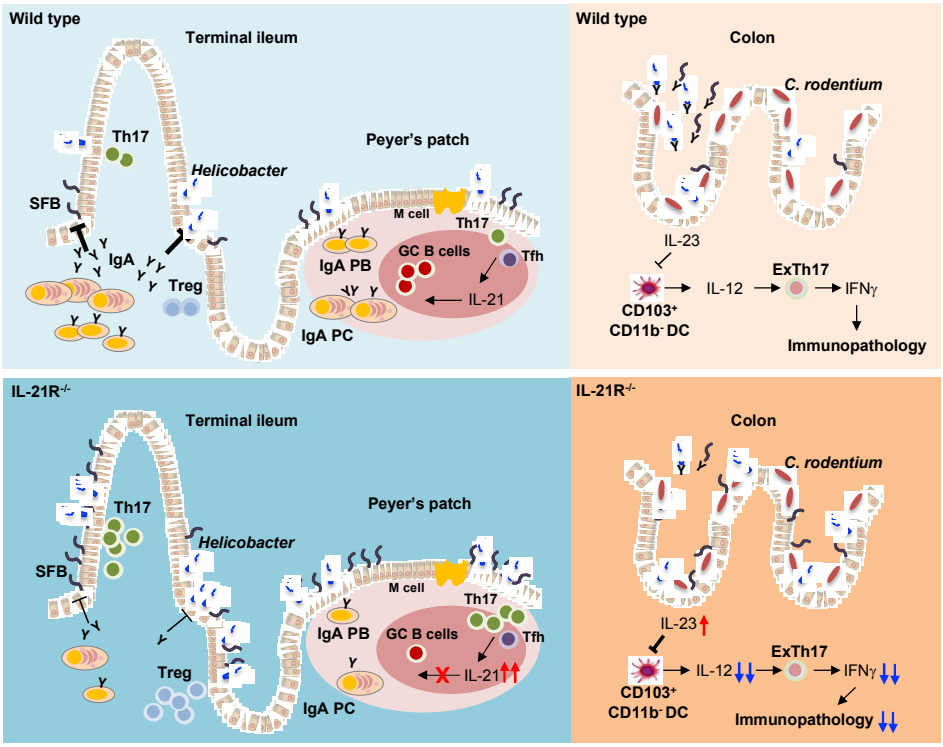

Supplementary Figure 8. A simplified working model of how IL-21 signaling contributes to intestinal homeostasis and immunity to *C. rodentium*. IL-21 is highly produced in Peyer's patches and the small intestinal lamina propria mainly by Tfh and Th17 cells. The presence of SFB enhances IL-21 production likely via expansion of IL-21-producing Th17 cells. IL-21 signaling is important for maintaining the optimal number of germinal center (GC) B cells and for promoting high-affinity T cell-dependent IgA class switching in Peyer's patches (PP) during homeostasis. The high-affinity T cell-dependent IgA response is essential for limiting atypical commensals/pathobionts such as SFB and *Helicobacter typhlonius*, but not the majority of commensals. In the presence of SFB and *Helicobacter typhlonius*, IL-21R deficiency results in decreased IgA class switching in PPs and consequently low levels of IgA in the intestine. This leads to overgrowth of these atypical commensals and/or their increased contact with the intestinal epithelium, inducing several functional effects. In the small intestine, these microbiota-mediated changes promote expansion of Th17 and Treg cells and enhance Th17/Treg responses to oral antigens, while in the colon, these changes mediate the

suppression of IL-12 via increased IL-23 and consequent reduction in IFNγ-mediated immunopathology following *Citrobacter rodentium* infection. PB and PC stand for plasmablasts and plasma cells.